AAS 15-799

OPTIMAL FORMATION DESIGN OF A MINIATURIZED DISTRIBUTED OCCULTER/TELESCOPE IN EARTH ORBIT

Adam W. Koenig[*], Simone D'Amico[†], Bruce Macintosh[‡], and Charles J. Titus[§]

This paper presents a novel formation design methodology for a miniaturized distributed occulter/telescope (mDOT) in earth orbit. In contrast to large-scale missions such as the New Worlds Observer or Exo-S (NASA), mDOT makes use of micro- and nano-satellites inertially aligned in earth orbit to reduce mission costs by orders of magnitude. Due to the small telescope aperture, this concept requires greater instrument integration time (or observation duration) in an environment with larger differential accelerations. As a consequence, a formulation of delta-v optimal absolute and relative orbits represents a mission enabler. The key contributions of this paper stem from the fundamental idea that the delta-v cost of observations can be optimized by allowing the formation to freely drift along the observation axis. First, this work presents an analytical expression of the delta-v cost of a pareto-optimal family of finite forced motion control maneuvers. Second, a method of selecting the initial argument of perigee and right ascension of the ascending node is presented that minimizes the deviation of the formation from its optimal configuration due to secular J_2 effects. Furthermore, it is demonstrated through high-fidelity numerical simulations that the delta-v optimal configuration with respect to forced motion control is also globally delta-v optimal. Finally, these simulations are used to show that the total delta-v cost for a mission consisting of multiple observations of a single target is well within the capacity of current small satellite propulsion systems.

INTRODUCTION

The astrophysics community has shown increasing interest in detection and characterization of exoplanets in recent years. While initial discoveries used Doppler or barycenter offset methods, progress has been made with precise transit photometry measurements. Most notably, NASA's Kepler mission is now responsible for more than one thousand confirmed exoplanet discoveries.[1] The indirect methods used for most discoveries to date allow scientists to determine the mass, size, and temperature of a planet, but provide little information about its chemical composition. The necessary data for this level of characterization can only be acquired via direct imaging. Spectroscopy data collected from direct images would allow scientists to identify key biosignature gases such as oxygen, water, and carbon dioxide. Approaches to direct imaging of exoplanets can be divided into two broad classes: 1) internal coronagraphs with adaptive optics, and 2) distributed

[*] Ph.D. Candidate, Stanford University, Department of Aeronautics & Astronautics, Space Rendezvous Laboratory, Durand Building, 496 Lomita Mall Stanford, CA 94305

[†] Assistant Professor, Stanford University, Department of Aeronautics & Astronautics, Space Rendezvous Laboratory, Durand Building, 496 Lomita Mall Stanford, CA 94305

[‡] Assistant Professor, Stanford University, Department of Physics, 382 Via Pueblo Mall, Stanford, CA 94305

[§] Ph.D. Candidate, Stanford University, Department of Physics, 382 Via Pueblo Mall, Stanford, CA 94305

occulter/telescope systems. Although internal coronagraphs in ground-based observatories have successfully imaged a few exoplanets,[2] these platforms are limited to instrument contrasts of 10^{-6} by atmospheric turbulence and instrument stability issues. Studies of space-based observatories suggest that these instruments can reach contrast levels of 10^{-10}, which would allow direct imaging of an earth analog. Although internal coronagraphs are being considered for spaceborne observatories (NASA Exo-C[3] and WFIRST-AFTA[4]), they are both expensive and complex.[5] Advances in formation flying technologies[6,7,8] in recent years suggest that the distributed occulter/telescope is a viable alternative to the internal coronagraph. A key advantage of this concept is that the occulter prevents the light from the star from ever reaching the telescope, negating the need for complex internal optics. Studies of the distributed occulter/telescope have resulted in several mission concepts including Exo-S (NASA)[9] and the New Worlds Observer (NWO) (NASA),[5] which aim to image multiple earth-like planets in the visible spectrum. The optical systems required to meet these objectives are extremely large. Specifically, these studies call for occulter diameters of tens of meters and baseline inter-spacecraft separations of tens of megameters. Due to the large baseline separation, the spacecraft are proposed to be deployed at Lagrange points instead of in earth orbit. The estimated cost of these missions is in the billions of dollars.

Considering the financial risk involved in development of a full-scale distributed occulter/telescope, it is desirable to first deploy a small-scale technology demonstrator. Such a mission would serve to 1) demonstrate the validity of the distributed occulter/telescope concept, 2) facilitate development of key enabling technologies for a full-scale system, and 3) directly image a small set of targets of scientific interest. In doing so, the technology demonstrator would increase confidence in the distributed occulter/telescope concept while providing a valuable science return. To that end, this paper describes a formation design methodology for a novel mission concept recently proposed by the authors,[10] namely a miniaturized distributed occulter/telescope (mDOT) consisting of two micro- or nano-satellites in earth orbit. The authors forsee an occulter of diameter no larger than $2\,\mathrm{m}$ separated from a $10\,\mathrm{cm}$ diameter telescope by several hundred kilometers. This occulter will be designed to suppress some specified bandwidth in the ultraviolet spectrum (specifically $150\text{-}400\,\mathrm{nm}$). Due to the optical challenges associated with imaging exoplanets on this scale, this mission aims instead to image exozodiacal dust disks. A novel feature of the proposed concept is that the spacecraft are allowed to drift along the line of sight during observations. Thus, the guidance, navigation, and control (GN&C) system need only counteract differential accelerations perpendicular to the line of sight.

Miniaturizing the distributed occulter/telescope to this degree introduces a number of challenges. First, formations in earth orbit are subject to larger differential accelerations than formations deployed near Lagrange points. Second, precision guidance, navigation, and control (GN&C) systems suitable for deployment on small satellites are presently at low technology readiness level. It is therefore evident that the delta-v cost associated with mission operations should be minimized in order the maximize the science return of a small-scale mission. To that end, this paper makes three key contributions to the state of the art. First, the authors develop an analytical formulation of the delta-v cost of a pareto-optimal family of finite forced motion control maneuvers that keep the formation aligned with a target star. This formulation is validated by comparing the analytical delta-v cost to simulations conducted using a geopotential model of order and degree 120. Second, an analytical method of selecting the argument of perigee and right ascension of the ascending node (RAAN) that minimizes the deviation of the formation from the optimal configuration over the expected mission lifetime due to secular J_2 effects is presented. Third, it is demonstrated through high-

fidelity numerical simulations that the cost associated with impulsively reconfiguring the formation between observations is small compared to the delta-v cost of forced motion control maneuvers in sub-optimal configurations. Finally, this orbit design strategy is implemented in a high-fidelity simulation of a mission to image Beta Pictoris (distance: 19 pc, visual magnitude: 3.86). This simulation demonstrates that the delta-v cost associated with imaging a target of scientific interest is well within the delta-v capacity of small satellite propulsion systems.

SCIENCE TARGET MODELING

Although a properly designed external occulter can almost perfectly block out the light from a star, one key obstacle must be addressed to image an exoplanet. Planets are intrinsically very faint. A jupiter analog orbiting even the nearest stars has a visual magnitude of 23 or fainter. This corresponds to a flux of 0.001 photons per second per centimeter squared. This signal is extremely difficult to detect with small telescopes. Even if the occulter perfectly blocks the host star, detector noise and Poisson noise from the background zodiacal light in our solar system and possibly the zodiacal analog in the target system can swamp the planetary signal. Figure 1 (left) shows the exposure time needed for a 5-sigma detection of a hypothetical planet orbiting the bright star Vega at 3.5 AU (corresponding to a 500 mas inner working angle), given the parameters in Table 1 for a range of telescope diameters. These exposure times are clearly impractical for all but the largest telescopes considered. There are some stellar targets that are slightly more favorable (e.g. Alpha Centauri), but these generally have other complications (e.g. Alpha Centauri is a binary star and there is no Doppler evidence for a Jovian planet present.) Statistics from existing Doppler surveys indicate that Jupiter-sized planets are rare with 2% of stars having a giant planet between 0.3 and 3 AU, so a survey that targets a few stars will likely not discover anything. The one possible exception is the giant planet tentatively detected by Doppler shifts orbiting the star Epsilon Eridani.[11] But since Epsilon Eridani is a fainter, redder star, exposure times would be approximately 12 times longer than those in Figure 1 (left). Exoplanet detection remains an interesting science driver for medium-sized telescopes but impractical for small telescopes.

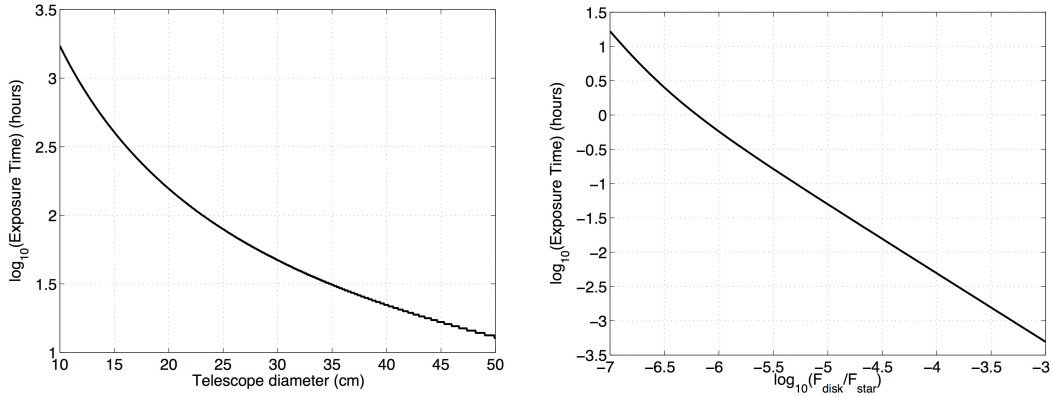

Figure 1. Necessary exposure time for 5-sigma detection of hypothetical planet using fiducial telescope model vs aperture diameter (left) and necessary exposure time for detection of hypothetical exozodiacal dust disk vs fractional brightness (right)

However, extrasolar planets are not the only high-contrast imaging targets of interest around nearby stars. In addition to its planetary system, our sun is orbited by asteroids and comets. Colli-

Table 1. Fiducial telescope model

Bandpass	200-300 nm
Throughput of camera	79%
QE of detector	80%
read noise	3 e^-/pixel
Dark current	0.0016 e^-/(pixel sec)

sions and erosion of these bodies produces the zodiacal dust. This both scatters sunlight and re-emits absorbed sunlight in the thermal infrared. The integrated light from zodiacal dust is actually a hundred times brighter than Jupiter - in our solar system, the flux due to dust is $F_{disk}/F_{star} = 10^{-7}$ of the luminosity of the sun. Similar disks have been detected around many nearby stars through this thermal emission, which is observed as excess infrared flux compared to the predicted stellar spectrum (the Vega phenomenon). These detections show that for many stars the total mass of dust is much higher than in our solar system, with F_{disk}/F_{star} as high as 10^{-3}. In most cases, the dust disk has been detected only through thermal emission at long wavelengths. Visible or near-infrared scattered light has been seen in some favorable cases (e.g. Beta Pictoris) with coronagraphy, but detecting the scattered light from these disks would be scientifically extremely interesting. Comparison of ultraviolet to visible to infrared brightness would help constrain the size of the scattering particles, and polarization properties could even provide information about their shape.[12] Detecting these disks is therefore both practical and scientifically compelling. Figure 1 (right) shows exposure times needed to detect a disk with the same geometry as that orbiting Beta Pictoris for a 10-cm telescope as a function of F_{disk}/F_{star} for an assumed occulter contrast of 10^{-7}. Since in many cases it is possible to identify systems with $F_{disk}/F_{star} > 10^{-5}$ via infrared techniques,[13] it is possible to target the optimal systems in advance of a mission.

PROPOSED CONCEPT DESCRIPTION

It is evident from the discussion in the previous section that while bright targets will only require short exposure times, more interesting targets may require tens of hours of integration time to detect. Considering the limits of small satellite GN&C systems, conducting such a long observation in one continuous pass in earth orbit is highly impractical. The proposed mDOT operations concept is designed to minimize the delta-v cost and maximize the science return of a small-scale mission. The envisioned mission operations strategy includes two phases: 1) a science phase during which a low-thrust, continuous control system is used to maintain decimeter-level relative position control while the telescope instrument images the target from within the shadow of the occulter, and 2) a reconfiguration phase during which the formation is reconfigured by a sequence of impulsive maneuvers to ensure proper alignment at the start of the next science phase. This operations strategy is inspired by the European Space Agency's PROBA-3 solar coronagraph concept,[14] but is subject to several distinct challenges. First, the baseline separation of the mDOT concept is several hundred kilometers, orders of magnitude larger than the PROBA-3 baseline. Additionally, the mDOT concept is subject to the onboard resource limitations of small satellites. The proposed operations concept is illustrated in Figure 2.

It has been demonstrated by the authors that it is possible to design a small occulter capable of achieving sufficient contrast to image exozodiacal dust disks over a small range of separation

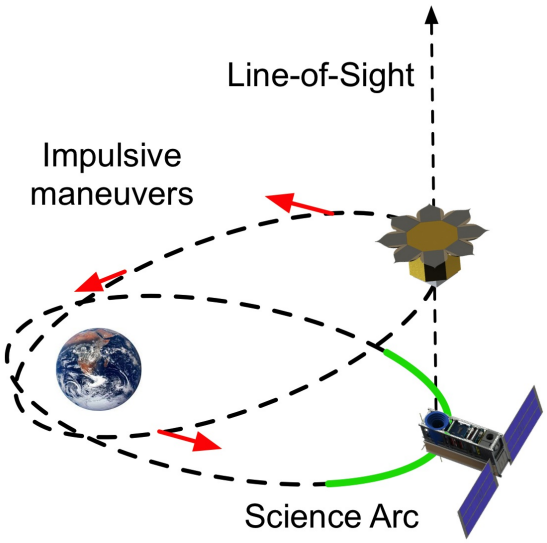

Figure 2. Illustration of telescope and occulter orbits (not to scale) noting quasi-continuous alignment control during the science phase (green) and impulsive control during the reconfiguration phase (red)

distances[10] ($\pm 1\%$ of the baseline). The proposed concept exploits this insensitivity to separation by allowing the spacecraft to freely drift along the line of sight during observations. Thus, the GN&C system need only counteract differential accelerations perpendicular to the line of sight. It will be demonstrated in the following analysis that this 1% drift allowance is sufficient to allow continuous observations of up to one hour before optical requirements are violated, provided that the orbit radius is at least 30 000 km when the exposure is taken.

DIFFERENTIAL ACCELERATION STUDY

In order to properly model the delta-v cost of mDOT, we first assess the magnitude of the differential accelerations that affect a spacecraft formation in earth orbit due to different perturbations. As such a comparison is not readily available in literature, we present a compilation of these differential accelerations here. For spacecraft in high orbits, significant acceleration sources include spherical earth gravity, the J_2 and J_3 geopotential zonal harmonics, third body forces due to the sun and moon, and solar radiation pressure. Differential atmospheric drag is neglected because it can be avoided by ensuring that the spacecraft are always at high altitudes (e.g. > 1000 km). To compute the differential acceleration due to each of these sources, the following considerations are made:

1) The gravitational acceleration due to a spherical body is purely a function of the distance between the spacecraft and the central body, r, and the gravitational parameter of the central body, μ. Given a specified baseline, the differential acceleration between two spacecraft orbiting a spherical body is maximized when the separation vector is exactly aligned with the radial direction. In this case, the differential acceleration, δg_{sphere}, between two spacecraft separated by distance ρ is given by

$$\delta g_{sphere} = \mu\left(\frac{1}{r^2} - \frac{1}{(r+\rho)^2}\right) \tag{1}$$

2) The relative acceleration due to zonal geopotential harmonics depends on both the orbit radius and geocentric latitude, β, of the spacecraft. From Vallado,[15] the perturbation, G_2, of the geopotential due to J_2 is given by

$$G_2 = -\frac{3\mu J_2 R_E^2}{2r^3}\Big(\sin^2\beta - \frac{1}{3}\Big) \tag{2}$$

where R_E denotes the mean earth radius. The magnitude of G_2 is maximized when $\sin\beta = 1$. In this case, the expression of G_2 simplifies to

$$G_2 = -\frac{\mu J_2 R_E^2}{r^3} \tag{3}$$

The acceleration due to J_2, denoted g_{J_2}, computed by differentiating G_2 with respect to r, is given by

$$g_{J_2} = \frac{3\mu J_2 R_E^2}{r^4} \tag{4}$$

If the spacecraft are assumed to be aligned in the radial direction, the differential acceleration due to J_2, δg_{J_2} is given by

$$\delta g_{J_2} = 3\mu {R_E}^2 J_2\Big(\frac{1}{r^4} - \frac{1}{(r+\rho)^4}\Big) \tag{5}$$

The same procedure is followed to evaluate the effect of J_3. The perturbation of the spherical geopotential due to J_3, denoted G_3, is given in Vallado[15] by

$$G_3 = -\frac{\mu J_3 R_E^3}{2r^4}\Big(5\sin^3\beta - 3\sin\beta\Big) \tag{6}$$

This is maximized when $\sin\beta = 1$. In this case, the expression for G_3 simplifies to

$$G_3 = -\frac{\mu J_3 R_E^3}{r^4} \tag{7}$$

As before, the acceleration due to J_3, denoted g_{J_3}, is given by

$$g_{J_3} = \frac{4\mu J_3 R_E^3}{r^4} \tag{8}$$

and the differential acceleration, δg_{J_3}, for a formation aligned in the radial direction is given by

$$\delta g_{J_3} = 4\mu {R_E}^2 J_3\Big(\frac{1}{r^5} - \frac{1}{(r+\rho)^5}\Big) \tag{9}$$

3) The acceleration of a spacecraft due to solar radiation pressure, $g_{pressure}$, depends on the spacecraft size, mass, surface properties, and orientation. However, for modeling purposes it can be approximated by

$$g_{pressure} = \frac{PA}{m} \tag{10}$$

where P is the solar radiation pressure at a distance of 1 AU ($4.56\,\mu$Pa[16]), A is the exposed area of the spacecraft, and m is the mass of the spacecraft. For this analysis we assume a 6U CubeSat

with a mass of 10 kg and a maximum exposed area of approximately 600 cm^2. The differential acceleration is given by

$$\delta g_{pressure} = \Delta c \frac{PA}{m} \tag{11}$$

where Δc denotes a normalized difference in the ballistic properties of the satellites.

Figure 3 plots the magnitude of each of the significant differential accelerations against the baseline separation for formations in low earth orbit (LEO) and geosynchronous earth orbit (GEO). The figure includes Δc values of 2% and 100% in the solar radiation pressure computation to illustrate the effect of satellites with very similar and different ballistic properties, respectively.

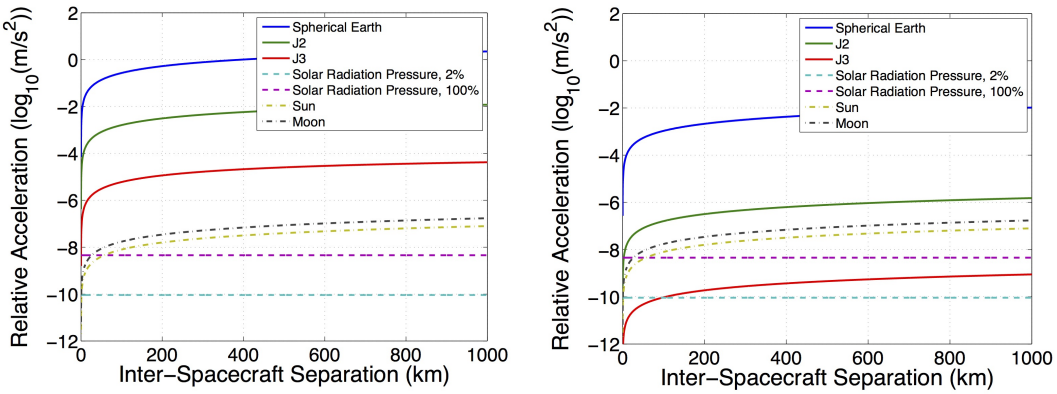

Figure 3. Magnitude of relative motion perturbations for LEO (left) and GEO (right) orbits

Several key conclusions can be drawn from Figure 3. First, it is evident that the differential acceleration decreases with increasing orbit radius. It follows that the delta-v cost associated with forced motion control is minimized if the orbit radius is maximized. Second, the spherical component of earth gravity is several orders of magnitude larger than all other perturbations regardless of inter-spacecraft separation and orbit radius. Hence, analysis of the cost of a single forced motion control maneuver includes only the spherical component of earth gravity. Finally, although the effect of J_2 is small compared to spherical earth gravity, this perturbation is known to introduce a secular drift in the orbit which must be addressed in order to minimize the delta-v cost of the entire mission over multiple orbits.

SCIENCE PHASE COST MODELING

The proposed mission operations strategy minimizes the delta-v cost associated with forced motion control by allowing the spacecraft to freely drift along the line of sight, requiring the GN&C system to only counteract differential accelerations perpendicular to the line of sight. It is therefore desirable to configure the formation during the science phase such that the differential acceleration acts along the line of sight. It will be demonstrated in the following analysis that ensuring that the formation is configured in this way for the duration of a multi-orbit mission fully constrains the formation design. First, an analytical formulation of the magnitude of the differential acceleration perpendicular to the line of sight is presented. It is found from this formulation that there exist formation configurations such that the relative acceleration due to spherical earth gravity is precisely aligned with the line-of-sight. Next, an analytical formula for the delta-v cost of a finite maneuver is developed by integrating this cost function subject to the constraint that the formation maintains

constant inertial alignment. Finally, a method is presented to select the initial orbit of the formation such that the deviation of the formation from the optimal configuration over the expected mission lifetime due to secular J_2 effects is minimized.

Instantaneous Cost Modeling

Figure 4 illustrates the mDOT formation in earth orbit with relevant design variables. In this model the inertial position and velocity vectors of the telescope are expressed by $\boldsymbol{r}$ and $\boldsymbol{v}$, respectively. A rotating orbit frame (RTN) centered at the telescope is defined by the radial (R, along $\boldsymbol{r}$), cross-track (N, along orbit normal), and along-track (T, completes right-handed triad) directions. The relative position vector of the occulter in the RTN frame, $\boldsymbol{\rho}$, can be decomposed into component displacements x, y, and z in the R, T, and N directions, respectively. Using this model, the

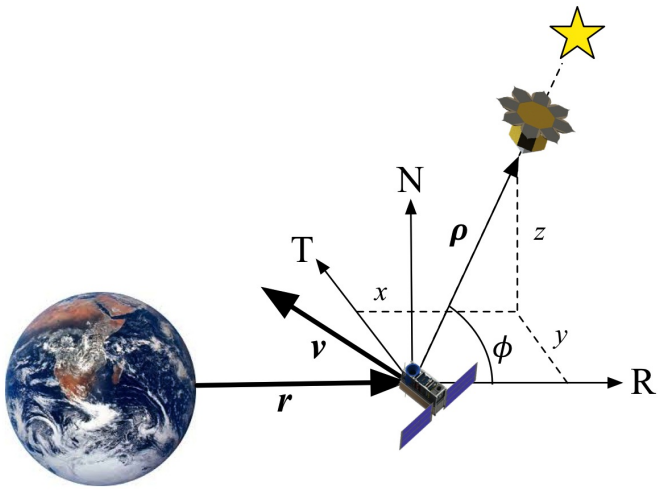

Figure 4. Illustration of mDOT formation in earth orbit (Not to scale) with relevant design variables

inertial gravitational accelerations of the telescope and occulter spacecraft, denoted $\boldsymbol{g}_{tel}$ and $\boldsymbol{g}_{occ}$, respectively, are given in the RTN frame by

$$\boldsymbol{g}_{tel} = -\frac{\mu \boldsymbol{r}}{||\boldsymbol{r}||^3} = -\mu \begin{bmatrix} \frac{1}{r^2} \\ 0 \\ 0 \end{bmatrix} \qquad \boldsymbol{g}_{occ} = -\frac{\mu(\boldsymbol{r}+\boldsymbol{\rho})}{||\boldsymbol{r}+\boldsymbol{\rho}||^3} = -\mu \begin{bmatrix} \frac{r+x}{\left((r+x)^2+y^2+z^2\right)^{3/2}} \\ \frac{y}{\left((r+x)^2+y^2+z^2\right)^{3/2}} \\ \frac{z}{\left((r+x)^2+y^2+z^2\right)^{3/2}} \end{bmatrix} \tag{12}$$

The relative acceleration due to spherical earth gravity, $\delta \boldsymbol{g}$, is simply the difference between these accelerations and is given by

$$\delta \boldsymbol{g} = \mu \begin{bmatrix} \frac{1}{r^2} - \frac{r+x}{\left((r+x)^2+y^2+z^2\right)^{3/2}} \\ -\frac{y}{\left((r+x)^2+y^2+z^2\right)^{3/2}} \\ -\frac{z}{\left((r+x)^2+y^2+z^2\right)^{3/2}} \end{bmatrix} \tag{13}$$

The component of this acceleration orthogonal to the line-of-sight, $\delta g_\perp$, is computed by taking the norm of the difference between $\delta \boldsymbol{g}$ and its projection onto $\boldsymbol{\rho}$, as given by

$$\delta g_\perp = ||\delta \boldsymbol{g} - \frac{\delta \boldsymbol{g} \cdot \boldsymbol{\rho}}{||\boldsymbol{\rho}||}\boldsymbol{\rho}|| = \mu\sqrt{\frac{y^2+z^2}{x^2+y^2+z^2}}\Big[\frac{r}{((r+x)^2+y^2+z^2)^{3/2}} - \frac{1}{r^2}\Big] \tag{14}$$

Using the identities $\rho = \sqrt{x^2+y^2+x^2}$ and $\phi = \arccos(x/\rho)$, which can be derived from Figure 4, Eq. (14) can be simplified to

$$\delta g_\perp = \mu \sin\phi\Big[\frac{r}{(r^2+2r\rho\cos\phi+\rho^2)^{3/2}} - \frac{1}{r^2}\Big] \tag{15}$$

It can be seen that the instantaneous cost varies strongly with the orbit radius. It follows that the semi-major axis of the orbits on the spacecraft should be as large as possible in order to minimize delta-v costs.

Additionally, inspection of Eq. (15) reveals that there exist two non-trivial conditions that reduce $g_\perp$ to zero. The first condition is given by $\phi = 0$, which corresponds to a formation aligned with the radial direction, R. However, because the relative velocity between the spacecraft during an observation must be small, it is evident that spacecraft aligned in the radial direction will have different mechanical energies. It follows that these formations are characterized by a large difference in semi-major axis. In order to perform periodic observations, it is necessary to remove and re-establish this baseline between science phases. The authors have found from simulations that the delta-v cost of these maneuvers is impractically large. As such, detailed forced motion control models of these formations are not discussed.

The second and more interesting condition that reduces $\delta g_\perp$ to zero occurs when $\phi = \arccos(-\rho/2r)$, which corresponds to a formation characterized by equal radii of the telescope and occulter orbits. Equivalently, this second condition corresponds to a formation aligned with the along-track/cross-track, TN, plane defined through curvilinear coordinates.[15] Families of configurations that satisfy this condition are illustrated in Figure 5 for different values of ρ and an orbit radius of $40\,000$ km. It can be seen that the radial component of the relative position vector is very small even for separations as large as 1000 km. As a final note, this configuration is not consistent with the assumption presented in the perturbation study that the formation is aligned in the radial direction. As a result, it is likely that third body and solar radiation pressure forces play a larger role in formation behavior than indicated in Figure 3. However, analysis of these forces, which depend both on time and the properties of the spacecraft, is left to future work.

Drift Modeling

Because the proposed mission concept endeavors to reduce the delta-v cost associate with formation keeping by only correcting relative acceleration perpendicular to the line of sight, the spacecraft will tend to drift along the line-of-sight over the course of a science phase. Indeed, the resulting change in separation can be several kilometers for long observations. The authors have demonstrated that it is possible to design occulters on a size scale compatible with micro-satellites that are capable of imaging targets of scientific interest that are robust to deviations of inter-spacecraft separation of up to 1%.[10] It will now be demonstrated that this is a sufficient design envelope to allow observations of at least 1-hour provided the orbit radius during the science phase is at least $30\,000$ km. Let $\bar{\rho}$ denotes the baseline inter-spacecraft separation specified by the optical system.

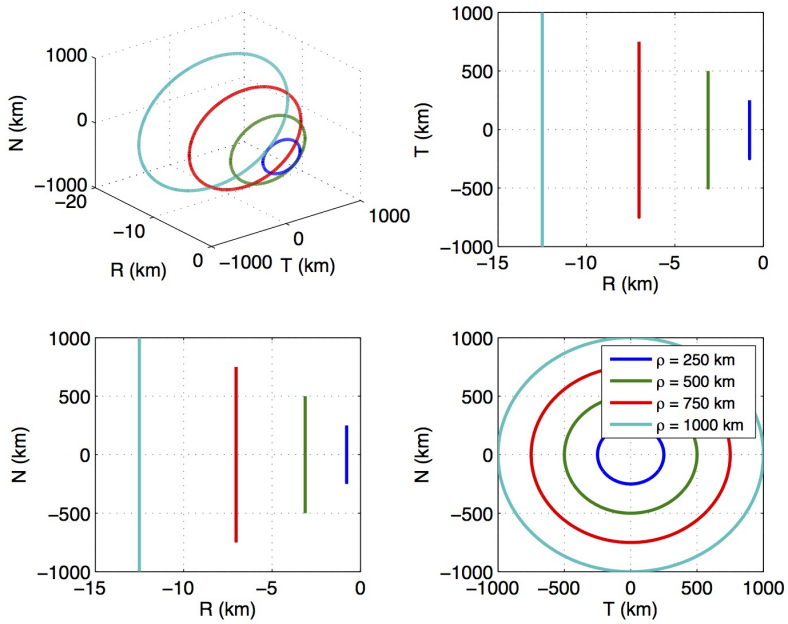

Figure 5. Families of zero cost configurations for orbit radius of 40 000 km

For two spacecraft with equal orbit radii, the differential acceleration along the line of sight, $\ddot{\rho}$, is computed from simple trigonometry according to

$$\ddot{\rho} = -2\frac{\mu}{r^2}\sin\left(\frac{\bar{\rho}}{2r}\right) \approx -\frac{\mu\bar{\rho}}{r^3} \tag{16}$$

If we assume that $\ddot{\rho}$ is constant over the duration of an observation, the time history of the inter-spacecraft separation can be modeled as a parabola, which is given by

$$\rho(t) = \rho(t_0) + \dot{\rho}(t_0)(t - t_0) + 0.5\ddot{\rho}(t - t_0)^2 \tag{17}$$

where $\rho(t)$ denotes the magnitude of the relative position vector at time t, $\dot{\rho}(t)$ denotes to the derivative with respect to time of $\rho(t)$, and t_0 denotes the start time of the science phase maneuver. It is desirable to minimize the maximum deviation of $\rho(t)$ from $\bar{\rho}$ over the course of an observation. This is the same as minimizing the difference between the maximum and minimum values of $\rho(t)$. Because the evolution of $\rho(t)$ is modeled as a parabola, its range is minimized if the initial and final values are equal. If the total maneuver duration is given by Δt, then the initial relative velocity $\dot{\rho}(t_0)$ must be selected to satisfy

$$\rho(t_0) = \rho(t_0 + \Delta t) = \rho(t_0) + \dot{\rho}(t_0)\Delta t - \frac{\mu\bar{\rho}}{2r^3}\Delta t^2 \tag{18}$$

Solving for $\dot{\rho}(t_0)$ yields

$$\dot{\rho}(t_0) = \frac{\mu\bar{\rho}\Delta t}{2r^3} \tag{19}$$

The optimal initial separation $\rho(t_0)$ is selected such that the deviation from $\bar{\rho}$ at the beginning and middle of the maneuver are equal. This condition is given by

$$\bar{\rho} - \rho(t_0) = \rho(t_0) + \frac{\dot{\rho}(t_0)\Delta t}{2} - \frac{\mu\bar{\rho}}{8r^3}\Delta t^2 - \bar{\rho} \tag{20}$$

Solving for $\rho(t_0)$ yields

$$\rho(t_0) = \bar{\rho}\Big(1 - \frac{\mu \Delta t^2}{16 r^3}\Big) \tag{21}$$

According to this model the maximum deviation normalized by the baseline separation is given by

$$\frac{\Delta\rho}{\bar{\rho}} = \frac{\mu \Delta t^2}{16 r^3} \tag{22}$$

Finally, if we assume the maximum allowable ratio $\Delta\rho/\bar{\rho}$ is fixed by the optical system, the maximum allowable observation time, denoted Δt_{max} is given by

$$\Delta t_{max} = \sqrt{\frac{16 r^3}{\mu} \frac{\Delta\rho}{\bar{\rho}}} \tag{23}$$

It can be seen that Δt_{max} depends only on the orbit radius and the drift tolerance of the optical system. Figure 6 illustrates the behavior of this bound over orbit radii from $10\,000$ to $45\,000$ km and maximum allowable drift fractions from zero to 5%. It can be seen that allowing ρ to drift by 1% is sufficient to ensure that a 1-hour long observation is achievable as long as the orbit radius is at least $30\,000$ km.

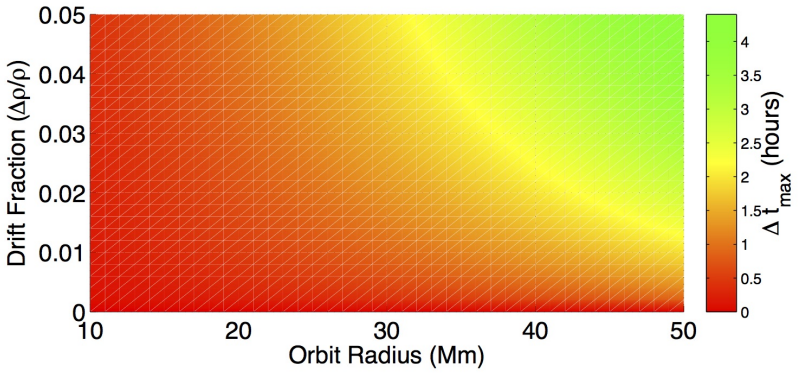

Figure 6. Maximum allowable observation time vs orbit radius and maximum allowable normalized drift

Finite Maneuver Cost Modeling

At this point, it has been established that there exist configurations such that the differential acceleration perpendicular to the line of sight is identically zero. It has also been demonstrated that it is possible to perform continuous maneuvers of at least 1-hour duration provided that the orbit radius is at least $30\,000$ km when the maneuver is performed. It is now possible to compute the delta-v cost associated with a finite maneuver. From Eq. (15), the delta-v cost of a finite forced motion control maneuver, denoted $\Delta v_{science}$, is given by

$$\Delta v_{science} = \int_{t_0}^{t_0+\Delta t} |g_\perp(t)| dt \tag{24}$$

It has been established that there exist configurations such that the value of $g_\perp$ is zero. The total delta-v cost of a finite maneuver can be minimized by selecting the maneuver such that $g_\perp(t_0 +$

$\Delta t/2) = 0$. This serves to minimize the maximum deviation from the zero-cost configurations. The evolution of $g_\perp$ can be linearized about such a point according to

$$g_\perp(t) = \frac{Dg_\perp}{Dt}\Big(t - t_0 - \frac{\Delta t}{2}\Big) \tag{25}$$

where $Dg_\perp/Dt$ denotes the substantial derivative of the instantaneous cost evaluated at $t = t_0 + \Delta t/2$. The general form of the substantial derivative is given by

$$\frac{Dg_\perp}{Dt} = \frac{\delta g_\perp}{\delta r}\frac{dr}{dt} + \frac{\delta g_\perp}{\delta \rho}\frac{d\rho}{dt} + \frac{\delta g_\perp}{\delta \phi}\frac{d\phi}{dt} \tag{26}$$

This expression can be greatly simplified considering the previous results of this work. It is known from classical Keplerian mechanics[15] that the time rate of change of the orbit radius at the apogee of an eccentric orbit (corresponding to the maximum orbit radius) or anywhere in a circular orbit is zero. Thus, the r-dependent terms of the substantial derivative can be neglected. Additionally, using the previously described parabolic model of the spacecraft drift, the time rate of change of ρ evaluated at $\Delta t/2$ is zero. Thus, the ρ-dependent terms can also be neglected. Thus, the simplified substantial derivative of the instantaneous cost is given by

$$\frac{Dg_\perp}{Dt} = \frac{\delta g_\perp}{\delta \phi}\frac{d\phi}{dt} \tag{27}$$

which depends only on the behavior of ϕ. The time evolution of ϕ depends on the evolution of the pointing vector to an inertial target in the RTN frame. This pointing vector is a function of the classical Keplerian orbit elements including ν, ω, i, and Ω. The transformation between the earth-centered inertial (ECI) and RTN frames is given by the following sequence of elementary rotation matrices

$$\hat{\boldsymbol{\rho}}^{RTN} = \boldsymbol{R}_3(\nu)\boldsymbol{R}_3(\omega)\boldsymbol{R}_1(i)\boldsymbol{R}_3(\Omega)\hat{\boldsymbol{\rho}}^{ECI} \tag{28}$$

where $\boldsymbol{R}_i$ denotes a rotation about the i^{th} axis. The formulae for the elementary rotation matrices are included in Appendix A. With the exception of true anomaly, the orbit elements evolve very slowly and only due to forces other than spherical earth gravity. For simplicity, the slowly varying terms are grouped in a vector defined by

$$\hat{\boldsymbol{\rho}}^{PQR} = R_3(\omega)R_1(i)R_3(\Omega)\hat{\boldsymbol{\rho}}^{ECI} = \begin{bmatrix} \sqrt{1-\gamma^2}\cos\nu^* \\ \sqrt{1-\gamma^2}\sin\nu^* \\ \gamma \end{bmatrix} \tag{29}$$

where $\hat{\boldsymbol{\rho}}^{PQR}$ represents the pointing vector to the target expressed in perifocal coordinates. In this relation, as illustrated in Figure 7, ν^* denotes the phase angle of the projection of the pointing vector onto the orbit plane and γ denotes the cross-track component of the pointing vector. This parameterization of the pointing vector, is selected in order to simplify the following formulations. Substituting Eq. (29) in Eq. (28) yields

$$\hat{\boldsymbol{\rho}}^{RTN} = \rho\, R_3(\nu)\begin{bmatrix} \sqrt{1-\gamma^2}\cos\nu^* \\ \sqrt{1-\gamma^2}\sin\nu^* \\ \gamma \end{bmatrix} = \rho\begin{bmatrix} \sqrt{1-\gamma^2}\cos(\nu^*-\nu) \\ \sqrt{1-\gamma^2}\sin(\nu^*-\nu) \\ \gamma \end{bmatrix} \tag{30}$$

which parameterizes the evolution of the pointing vector as a function of ν, ν^*, and γ. From

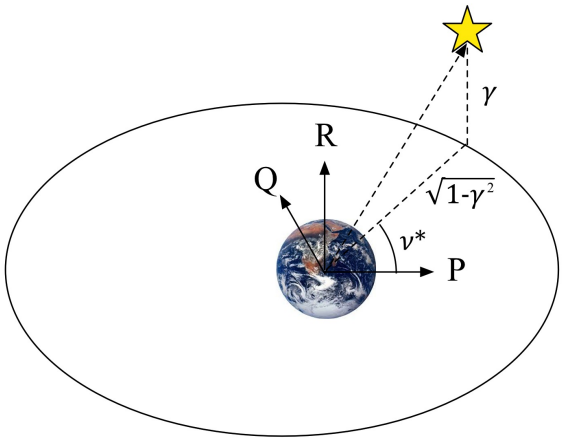

Figure 7. Illustration of the pointing vector to the target expressed in perifocal coordinates

Eq. (30) it is clear that the motion of the pointing vector to an inertial target is characterized by a circle in the radial/along-track plane with a constant offset in the cross-track direction. This has immediate consequences on the cost of finite maneuvers. Consider the shape of the surface that satisfies $\delta g_\perp = 0$ as illustrated in Figure 5. This surface is characterized by circles in the along-track/cross-track plane with a constant, small offset in the anti-radial direction which depends on the inter-spacecraft separation. To asses the cost associated with finite maneuvers, consider the states in which the radial component of the pointing vector as defined by Eq. (30) is small. There are two broad classes of states that satisfy this condition. First, the radial component of the pointing vector is small if $\cos(\nu^* - \nu) \approx 0$. However, if $|\gamma|$ is small, the radial component of the vector changes rapidly as ν evolves. Thus, the pointing vector will be far removed from the instantaneous zero-cost configurations. The second class of states where the radial component of the relative position is small is defined by $|\gamma| \approx 1$. In these cases, the pointing vector lies almost entirely in the cross-track direction. Consequently, the radial component of the pointing vector is always small, ensuring that the formation is always near the instantaneous zero-cost configurations. It is therefore evident that the delta-v cost associated with a finite forced-motion control maneuver is minimized if the formation points in the cross-track direction. Equivalently, the delta-v cost is minimized by maximizing $|\gamma|$. For clarity, Figure 8 illustrates the evolution of the relative position vector in the RTN frame of an mDOT formation in a circular orbit of $40\,000$ km radius with a 500 km baseline separation if 1-hour long observations are performed for various values of $|\gamma|$. These maneuvers are centered about the instantaneous zero-cost configurations defined by Eq. (15), which are denoted by the green surface in the figure. It can be clearly seen that the maximum distance from the instantaneous zero-cost surface increases with decreasing$|\gamma|$.

Now that the evolution of the pointing vector to the target has been characterized, the substantial derivative of $\delta g_\perp$ can be evaluated. Because ϕ is the angle between the pointing vector to the target and the radial direction, it can be expressed as a function of ν and γ by substituting the radial component of Eq. (30). This expression is given by

$$\cos\phi = \sqrt{1-\gamma^2}\cos(\nu^* - \nu) \tag{31}$$

Because ϕ is written as a function of ν, the substantial derivative given in Eq. (27) can be expanded

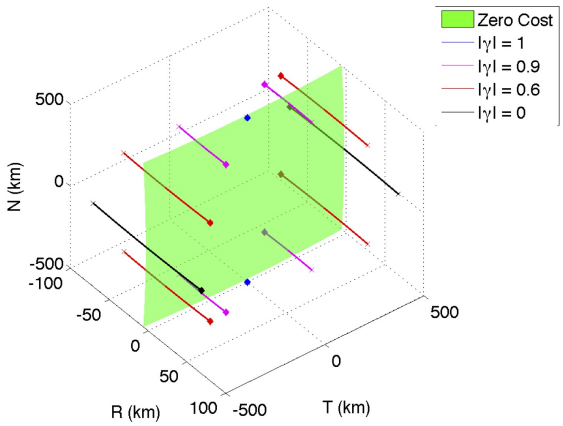

Figure 8. Deviation from instantaneous zero-cost surface of RTN position tracks for various values of $|\gamma|$

by applying the chain rule, which yields

$$\frac{Dg_\perp}{Dt} = \frac{\delta g_\perp}{\delta \phi}\frac{d\phi}{d\nu}\frac{d\nu}{dt} \tag{32}$$

From Eq. (15), the partial derivative of $g_\perp$ with respect to ϕ is given by

$$\frac{dg_\perp}{d\phi} = \mu\Big(\cos\phi\Big[\frac{r}{(r^2+2r\rho\cos\phi+\rho^2)^{1.5}} - \frac{1}{r^2}\Big] + \frac{3r^2\rho\sin^2\phi}{(r^2+2r\rho\cos\phi+\rho^2)^{2.5}}\Big) \tag{33}$$

Evaluating at $\cos\phi = -\rho/(2r)$ yields

$$\frac{dg_\perp}{d\phi} = \frac{3\mu\rho}{r^3}\Big(1-\frac{\rho^2}{4r^2}\Big) \tag{34}$$

From Eq. (31), the derivative of ϕ with respect to ν is given by

$$\frac{d\phi}{d\nu} = \frac{\sin(\nu^*-\nu)}{\sqrt{(1-\gamma^2)\sin^2(\nu^*-\nu)+\gamma^2}} \tag{35}$$

Additionally, solving Eq. (31) for ν at the optimal observation point yields

$$\cos(\nu^*-\nu) = -\frac{\rho}{\sqrt{2r(1-\gamma^2)}} \tag{36}$$

Substituting Eq. (36) into Eq. (35) yields

$$\frac{d\phi}{d\nu} = \frac{\sqrt{1-\gamma^2-\frac{\rho^2}{4r^2}}}{\sqrt{1-\frac{\rho^2}{4r^2}}} \tag{37}$$

The time rate of change of ν from classical Keplerian mechanics[15] is given as a function of a and e by

$$\frac{d\nu}{dt} = \frac{\sqrt{\mu a(1-e^2)}}{r^2} \tag{38}$$

Combining Eqs. (32), (34), (35), and (38) yields

$$\frac{Dg_{\perp}}{Dt} = \frac{3\mu\rho}{r^5}\sqrt{\mu a(1-e^2)\Big(1-\frac{\rho^2}{4r^2}\Big)\Big(1-\gamma^2-\frac{\rho^2}{4r^2}\Big)} \tag{39}$$

Finally substituting Eq. (25) and Eq. (39) into Eq. (24) yields

$$\Delta v_{science} = \int_{t_0}^{t_0+\Delta t}(t-t_0-\frac{\Delta t}{2})\frac{3\mu\rho}{r^5}\sqrt{\mu a(1-e^2)\Big(1-\frac{\rho^2}{4r^2}\Big)\Big(1-\gamma^2-\frac{\rho^2}{4r^2}\Big)}dt \tag{40}$$

which can be evaluated directly. The resulting delta-v cost is given by

$$\Delta v_{science} = \frac{3\mu\rho\Delta t^2}{4r^5}\sqrt{\mu a(1-e^2)\Big(1-\frac{\rho^2}{4r^2}\Big)\Big(1-\gamma^2-\frac{\rho^2}{4r^2}\Big)} \tag{41}$$

Eq. (41) presents an analytical expression for the delta-v cost associated with a finite forced motion control maneuver to achieve constant inertial pointing. This expression was developed by integrating an analytical expression of the differential acceleration perpendicular to the line of sight due to spherical earth gravity. There are three key assumptions used in this derivation: 1) The maneuver is centered about a configuration where the instantaneous cost as defined by Eq. (15) is zero, 2) the orbit radius is constant during the maneuver, and 3) the inter-spacecraft separation is constant during the maneuver. There are a number of important conclusions that can be drawn from Eq. (41). First, in a consistent manner with Eq. (15), the delta-v cost depends very strongly on the orbit radius. Thus, the orbit semi-major axis should be maximized in order to minimize cost. Second, increasing the eccentricity of the orbit reduces the delta-v cost of the forced motion control maneuver. Indeed, if the maneuver is performed at the apogee, an increase in eccentricity corresponds to an increase in the orbit radius, reducing the delta-v cost. Third, the total cost depends on the parameter γ, which is an analog of the cross-track component of the relative position vector. Indeed, configurations that satisfy $\gamma^2 = 1-\rho^2/(4r^2)$ have a delta-v cost of zero to first order. Following from Eq. (30), maximizing $|\gamma|$ requires that the pointing vector to the target is perpendicular to the orbit plane. There are two sets of i and Ω that satisfy $|\gamma| = 1$. These correspond to cases where the orbit angular momentum vector is either parallel or anti-parallel to the pointing vector to the target, respectively. It should be noted that Eq. (41) only applies to orbits that satisfy $|\gamma| \leq \sqrt{1-\rho^2/(4r^2)}$. However, orbits that violate this constraint will remain very close to the instantaneous zero-cost configurations.

To illustrate the behavior of the delta-v cost presented in Eq. (41), Figure 9 (left) illustrates the behavior of $\Delta v_{science}$ for 1-hour long observations for an mDOT formation in a circular orbit with a $500\,\text{km}$ baseline separation for a range of orbit semi-major axis and γ values. It can be seen that unless the formation has a very high value of $|\gamma|$, it is essential that the orbit be as large as possible. To validate the assumptions used in the derivation of Eq. (41), Figure 9 (right) compares the delta-v cost as from the analytical formula with the delta-v cost computed from high-fidelity numerical simulations with the GRACE Gravity model GGM01S of degree and order 120[17] for a formation with a $40\,000\,\text{km}$ orbit radius for various values of γ. It can be seen that the analytical model agrees with simulation results to within 1%.

Secular J_2 Effects

We have thus far established that minimizing the delta-v cost associated with forced-motion control maneuvers imposes three key constraints on the orbit: 1) the orbit semi-major axis should be

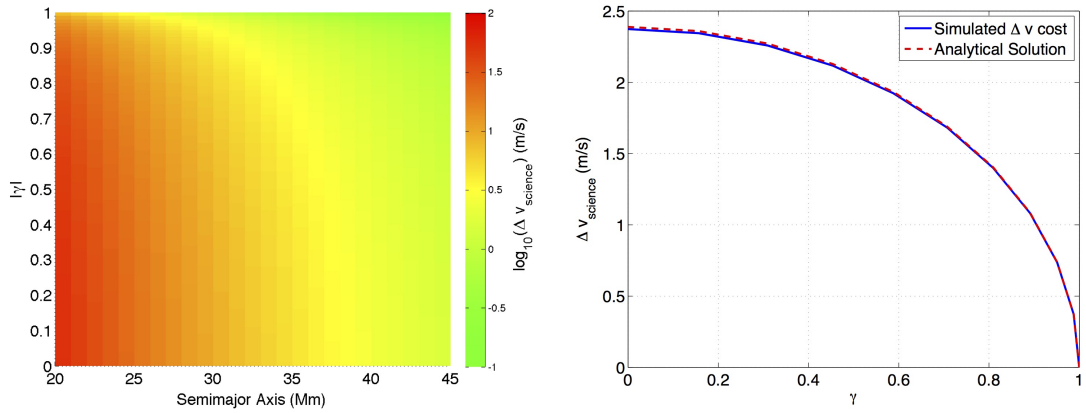

Figure 9. Optimal science phase delta-v cost for 1-hour observations in a circular orbit vs a and γ (left) and comparison with simulation (right)

maximized in order to achieve a large orbit radius, 2) the eccentricity of the orbit should be maximized, provided that the science phase can be conducted at the apogee, and 3) the formation should be configured such that the angular momentum vector of the telescope orbit is either parallel or anti-parallel with the pointing vector to the target. However, these considerations were developed under the assumption that the orbit elements were constant. In order to fully minimize the delta-v cost of a multi-orbit mission, it is necessary to account for effects of the secular drift of the argument of perigee and RAAN due to J_2. Following from the assumptions used to develop Eq. (41), the argument of perigee and RAAN should be selected with two considerations in mind: 1) the maximum difference between the angular momentum vector of the orbit and the pointing vector to the target over the expected mission lifetime should be minimized, and 2) the pointing vector to the target at the science phase location (e.g. the apogee of an eccentric orbit) should closely follow the TN-plane. Before proceeding, it is first insightful to consider the conventional definition of the pointing vector to a star. The position of a star is frequently described by two angles: the right ascension, α, and declination, δ. From these angles, the pointing vector in the ECI frame, $\hat{\boldsymbol{\rho}}^{ECI}$, is given by

$$\hat{\boldsymbol{\rho}}^{ECI} = \begin{bmatrix} \cos\alpha\cos\delta \\ \sin\alpha\cos\delta \\ \sin\delta \end{bmatrix} \tag{42}$$

Recall from Eq. (28) that the pointing vectors expressed in the RTN and ECI frames are related by an elementary sequence of rotations. The alignment between the angular momentum of the orbit and the pointing vector to the target depends only on i and Ω. Consider an orbit with an argument of perigee and true anomaly of zero. Under this assumption, the pointing vector in the RTN frame is given by

$$\hat{\boldsymbol{\rho}}^{RTN} = \boldsymbol{R}_1(i)\boldsymbol{R}_3(\Omega)\hat{\boldsymbol{\rho}}^{ECI} = \begin{bmatrix} \cos\Omega & \sin\Omega & 0 \\ -\cos i\sin\Omega & \cos i\cos\Omega & \sin i \\ \sin i\sin\Omega & -\sin i\cos\Omega & \cos i \end{bmatrix} \begin{bmatrix} \cos\alpha\cos\delta \\ \sin\alpha\cos\delta \\ \sin\delta \end{bmatrix} \tag{43}$$

Combining the terms in this equation yields

$$\hat{\boldsymbol{\rho}}^{RTN} = \begin{bmatrix} \cos\delta(\cos\Omega\cos\alpha + \sin\Omega\sin\alpha) \\ \cos i\cos\delta(-\sin\Omega\cos\alpha + \cos\Omega\sin\alpha) + \sin i\sin\delta \\ \sin i\cos\delta(\sin\Omega\cos\alpha - \cos\Omega\sin\alpha) + \cos i\sin\delta \end{bmatrix} \tag{44}$$

which can be further simplified to yield

$$\hat{\boldsymbol{\rho}}^{RTN} = \begin{bmatrix} \cos\delta\cos(\alpha-\Omega) \\ \cos i\cos\delta\sin(\alpha-\Omega)+\sin i\sin\delta \\ -\sin i\cos\delta\sin(\alpha-\Omega)+\cos i\sin\delta \end{bmatrix} \tag{45}$$

The necessary and sufficient condition to align the pointing vector with the angular momentum vector is that the first two terms of this expression are zero. There are two solutions that meet this condition. The first solution is given by

$$\Omega = \alpha + \pi/2 \qquad i = -\delta + \pi/2 \tag{46}$$

The second solution is given by

$$\Omega = \alpha - \pi/2 \qquad i = \delta + \pi/2 \tag{47}$$

These solutions correspond to angular momentum vectors aligned parallel and anti-parallel, respectively, to the pointing vector to the target.

Consider the effect of a small change in the RAAN, denoted $\Delta\Omega$, on the pointing vector defined by Eq. (45) given by

$$\Delta\hat{\boldsymbol{\rho}}^{RTN} = \Delta\Omega \begin{bmatrix} \cos\delta\sin(\alpha-\Omega) \\ -\cos i\cos\delta\cos(\alpha-\Omega) \\ \sin i\cos\delta\cos(\alpha-\Omega) \end{bmatrix} \tag{48}$$

Substitution of the values from the solutions that align the angular momentum of the orbit with the pointing vector (Eqs. (46-47)) to the target yields

$$\Delta\hat{\boldsymbol{\rho}}^{RTN} = \begin{bmatrix} \pm\cos\delta\Delta\Omega \\ 0 \\ 0 \end{bmatrix} \tag{49}$$

We have thus far assumed that the argument of perigee and true anomaly are zero. It is now convenient to generalize this expression to compute the pointing vector in the RTN frame to the desired target at the apogee of an orbit for an arbitrary argument of perigee when the angular momentum vector is slightly misaligned with the target due to $\Delta\Omega$. This pointing vector is given by

$$\Delta\hat{\boldsymbol{\rho}}^{RTN} = \boldsymbol{R}_3(\omega+\pi) \begin{bmatrix} \pm\cos\delta\Delta\Omega \\ 0 \\ 0 \end{bmatrix} = \pm\cos\delta\Delta\Omega \begin{bmatrix} -\cos\omega \\ \sin\omega \\ 0 \end{bmatrix} \tag{50}$$

Finally, the resulting pointing vector to the target at the apogee is given by

$$\hat{\boldsymbol{\rho}}^{RTN} = \begin{bmatrix} \mp\cos\omega\cos\delta\Delta\Omega \\ \pm\sin\omega\cos\delta\Delta\Omega \\ 1 \end{bmatrix} \tag{51}$$

Eq. (51) describes the pointing vector to the target in the RTN frame at the apogee of an orbit where the angular momentum is misaligned with the target due to a RAAN perturbation. It can be seen that this misalignment introduces a component of the pointing vector in the RT-plane and the direction of this component depends on the argument of perigee. In order to ensure that the pointing vector

evolves in the TN-plane it is clear from Eq. (51) that the optimal values of the argument of perigee are $\omega = \pi/2$ or $\omega = 3\pi/2$.

The above considerations define the ideal values of the ω and Ω. Because J_2 causes a constant secular drift in these terms, the delta-v cost associated with J_2 effects is minimized by simply centering the argument of perigee and RAAN about these values over the expected mission lifetime. The secular drift of Ω in radians per second due to J_2, denoted $\dot{\Omega}$ is given by

$$\dot{\Omega} = -1.5J_2\Big(\frac{R_E}{a(1-e^2)}\Big)^2 n\cos i \tag{52}$$

where n is the mean motion of the orbit. The total change over the course of an orbit can be computed by multiplying by the orbit period, yielding

$$\Delta\Omega = -3\pi J_2\Big(\frac{R_E}{a(1-e^2)}\Big)^2 \cos i \tag{53}$$

Similarly, the secular drift of ω, denoted $\dot{\omega}$, is given by

$$\dot{\omega} = 0.75J_2\Big(\frac{R_E}{a(1-e^2)}\Big)^2 n(5\cos^2 i - 1) \tag{54}$$

and the change over a single orbit is given by

$$\Delta\omega = 1.5\pi J_2\Big(\frac{R_E}{a(1-e^2)}\Big)^2 (5\cos^2 i - 1) \tag{55}$$

Now, let Ω^* denote the desired solution that aligns the angular momentum vector of the telescope orbit with the pointing vector to the target. If the expected mission duration is N orbits, the ideal choice for the initial value of the RAAN, denoted Ω_0 is given by

$$\Omega_0 = \Omega^* - 0.5N\Delta\Omega \tag{56}$$

Similarly, if ω^* denote the desired value of the argument of perigee ($\pi/2$ or $3\pi/2$), then the optimal initial value of the argument of perigee, denoted ω_0, is given by

$$\omega_0 = \omega^* - 0.5N\Delta\omega \tag{57}$$

It is evident from the preceding analysis that the precession of the orbit due to J_2 depends on the inclination of the orbit, which is specified by the location of the science target of interest. Noting the dependence of the orbit alignment on Ω, one could conceive an operations strategy that uses a sequence of maneuvers to counteract $\dot{\Omega}$, ensuring that the absolute orbit of the formation is always optimal. However, implementation of this strategy incurs large delta-v costs when compared to the costs incurred by the presented formation design methodology for the vast majority of cases. The cost associated with counteracting the RAAN drift over a single orbit is computed from the Gauss variational equations[18] as given by

$$\Delta v = \frac{h\sin i}{r\sin\theta}\Delta\Omega \tag{58}$$

where h denotes the angular momentum of the orbit. If the maneuver is assumed to be performed at the apogee, this is given as a function of the semi-major axis, eccentricity, and inclination by

$$\Delta v = 1.5\pi J_2\sqrt{\frac{\mu(1-e)}{a(1+e)}}\Big(\frac{R_E}{a(1-e^2)}\Big)^2 \sin(2i) \tag{59}$$

To illustrate the behavior of this cost, Figure 10 shows the delta-v cost per orbit of correcting the RAAN drift for the orbit size and shape specified in Table 2 for an inclination range of 0 to 90^o. This cost is incurred once per orbit for the entire mission duration. It can be seen that the delta-v cost of correcting the RAAN drift of one spacecraft for a single orbit is larger than the worst-case science phase cost for the pareto-optimal maneuvers. Indeed, the cost of correcting the RAAN in a less favorable inclination for a single orbit is larger than the total mission cost using the proposed formation design strategy, as will be demonstrated later in high-fidelity simulations.

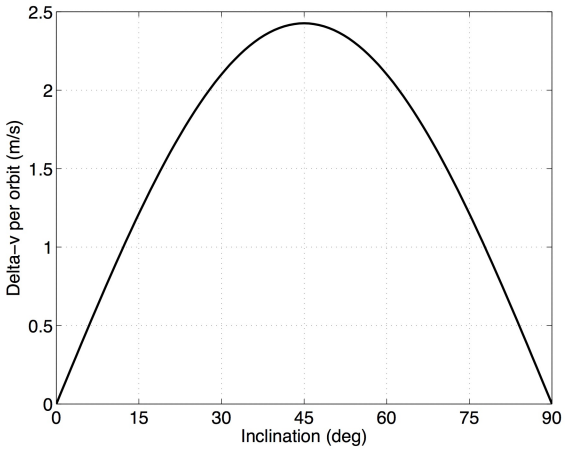

Figure 10. Plot of delta-v cost of correcting RAAN drift over single reference orbit vs inclination

RECONFIGURATION PHASE

At this stage we have not yet addressed how to reconfigure the formation between science phases. The maneuvers performed during the reconfiguration sequence, $\Delta \boldsymbol{v}_j$, must be selected to acquire the desired relative state at the start of the next science phase, $\delta \boldsymbol{\alpha}_f$, from the initial state obtained at the end of the previous science phase, $\delta \boldsymbol{\alpha}_i$. Following an approach similar to Gaias and D'Amico[19] and D'Amico and Montenbruck,[20] the evolution of the state vector over the reconfiguration phase can be expressed as

$$\delta \boldsymbol{\alpha}_f = \frac{1}{na} \sum \boldsymbol{\Phi}(M_j, M_f) \boldsymbol{B}_j \Delta \boldsymbol{v}_j + \boldsymbol{\Phi}(M_i, M_f) \delta \boldsymbol{\alpha}_i \tag{60}$$

where $\boldsymbol{\Phi}$ and $\boldsymbol{B}_j$ represent the state transition and control input matrices, which are discussed in the following. In order to extend the validity of the maneuver planning approach to eccentric orbits, the state vector of choice is a modified set of relative orbital elements (ROE) given by

$$\delta \boldsymbol{\alpha} = \begin{pmatrix} \delta a \\ \delta \lambda \\ \delta e_x \\ \delta e_y \\ \delta i_x \\ \delta i_y \end{pmatrix} = \begin{pmatrix} (a_c - a_d)/a_d \\ M_c - M_d + \eta(\omega_c - \omega_d + (\Omega_c - \Omega_d)\cos i_d) \\ e_c - e_d \\ \omega_c - \omega_d + (\Omega_c - \Omega_d)\cos i_d \\ i_c - i_d \\ (\Omega_c - \Omega_d)\sin i_d \end{pmatrix} \tag{61}$$

To obtain closed-form solutions for the impulsive maneuvers, the following state transition matrix is adopted for unperturbed eccentric orbits which accounts for the evolution of the relative mean

longitude over the mean anomaly interval $[M_i,\, M_f]$

$$\boldsymbol{\Phi}(M_i, M_f) = \begin{bmatrix} 1 & 0 & 0 & 0 & 0 & 0 \\ -1.5(M_i - M_f) & 1 & 0 & 0 & 0 & 0 \\ 0 & 0 & 1 & 0 & 0 & 0 \\ 0 & 0 & 0 & 1 & 0 & 0 \\ 0 & 0 & 0 & 0 & 1 & 0 \\ 0 & 0 & 0 & 0 & 0 & 1 \end{bmatrix} \tag{62}$$

The control matrix, $\boldsymbol{B}_j$, evaluated at the location of the j^{th} impulsive maneuver, is derived from the Gauss variational equations[18] as

$$\boldsymbol{B}_j = \begin{bmatrix} \frac{2e}{\eta}\sin\nu_j & \frac{2}{\eta}(1+e\cos\nu_j) & 0 \\ \frac{-2\eta^2}{1+e\cos\nu_j} & 0 & 0 \\ \eta\sin\nu_j & \eta\frac{(2+e\cos\nu_j)\cos\nu_j+e}{1+e\cos\nu_j} & 0 \\ -\frac{\eta}{e}\cos\nu_j & \frac{\eta}{e}\frac{(2+e\cos\nu_j)\sin\nu_j}{1+e\cos\nu_j} & 0 \\ 0 & 0 & \frac{\eta\cos\theta_j}{1+e\cos\nu_j} \\ 0 & 0 & \frac{\eta\sin\theta_j}{1+e\cos\nu_j} \end{bmatrix} \tag{63}$$

where $\theta = \nu + \omega$ denotes the true argument of latitude and $\eta = \sqrt{1-e^2}$.

Before describing the reconfiguration solution, it is insightful to first consider the effects of different perturbations on the relative state over the course of the reconfiguration phase. Let $\delta\boldsymbol{\alpha}_0$ denote the relative state at the start of the first science phase. This is related to the initial state of the reconfiguration phase (or final state of the science phase) by

$$\delta\boldsymbol{\alpha}_i = \delta\boldsymbol{\alpha}_0 + \Delta\delta\boldsymbol{\alpha}_{science} \tag{64}$$

where $\Delta\delta\boldsymbol{\alpha}_{science}$ denotes the change in the ROE due to control input during the science phase. Next, consider the behavior of the desired relative state, $\delta\boldsymbol{\alpha}_f$. If the absolute orbit were fixed, the desired state would be the same at the start of every science phase. However, because the RAAN and argument of perigee exhibit a secular drift due to J_2, the desired state must change between each science phase. If the change in the desired state due to the secular drift is denoted $\Delta\delta\boldsymbol{\alpha}_{J_2}$, then the relationship between the desired states at the start of subsequent science phases is given by

$$\delta\boldsymbol{\alpha}_f = \delta\boldsymbol{\alpha}_0 + \Delta\delta\boldsymbol{\alpha}_{J_2} \tag{65}$$

We can substitute Eqs. (64-65) into Eq. (60), which yields

$$\delta\boldsymbol{\alpha}_0 + \Delta\delta\boldsymbol{\alpha}_{J_2} = \frac{1}{na}\sum \boldsymbol{\Phi}(M_j, M_f)\boldsymbol{B}_j\Delta\boldsymbol{v}_j + \boldsymbol{\Phi}(M_i, M_f)(\delta\boldsymbol{\alpha}_0 + \Delta\delta\boldsymbol{\alpha}_{science}) \tag{66}$$

This relation can be simplified by isolating the reconfiguration maneuver terms as given by

$$\frac{1}{na}\sum \boldsymbol{\Phi}(M_j, M_f)\boldsymbol{B}_j\Delta\boldsymbol{v}_j = \Delta\delta\boldsymbol{\alpha}_{J_2} - \boldsymbol{\Phi}(M_i, M_f)\Delta\delta\boldsymbol{\alpha}_{science} - (\boldsymbol{\Phi}(M_i, M_f) - \boldsymbol{I})\delta\boldsymbol{\alpha}_0 \tag{67}$$

From Eq. (67), the required maneuvers in the reconfiguration phase derive from three sources: 1) control input during the science phase ($\Delta\delta\boldsymbol{\alpha}_{science}$), 2) evolution of the desired state due to secular

argument of perigee and RAAN drift ($\Delta\delta\boldsymbol{\alpha}_{J_2}$), and 3) differential effects due to J_2 and Keplerian mechanics.

The closed-form solution to the reconfiguration problem exploits the decoupling of the in-plane (δa, $\delta\lambda$, δe_x, and δe_y) and out-of-plane (δi_x and δi_y) ROE. The solution method uses one cross-track impulse to correct the relative inclination vector and a sequence of three tangential impulses to correct the in-plane ROE. The solution methodology proceeds as described by Gaias and D'Amico.[19] First, it can be seen from Eqs. (62) and (63) that it is possible to achieve an arbitrary change in the relative inclination vector from a single cross-track impulse applied at the proper location. The magnitude, Δv_{oop}, and true argument of latitude, θ_{oop}, of this maneuver are given by

$$\theta_{oop} = \arctan\left(\frac{\Delta\delta i_y}{\Delta\delta i_x}\right) + k\pi \qquad \Delta v_{oop} = \frac{na}{\eta}(1 + e\cos\nu_{oop})\sqrt{\Delta\delta i_x^2 + \Delta\delta i_y^2} \tag{68}$$

where k is an arbitrary integer. It can be seen from Eq. (68) that there are two maneuver locations per orbit that allow for an arbitrary change in the relative inclination vector. The cost of the out-of-plane reconfiguration is minimized by selecting the maneuver location that satisfies $\cos\nu_{oop} \leq 0$.

The solution to the in-plane reconfiguration problem proceeds as follows. It is possible to achieve an arbitrary change in the in-plane ROE state through a sequence of three tangential impulses provided that the maneuver locations are selected such that the realized and desired changes in the relative eccentricity vector are aligned. Accordingly, the true anomaly of each in-plane maneuver, ν_{ip}, must satisfy

$$\arctan\left(\frac{(2 + e\cos\nu_{ip})\sin\nu_{ip}}{e((2 + e\cos\nu_{ip})\cos\nu_{ip} + e)}\right) = \pm\arctan\left(\frac{\Delta\delta e_y}{\Delta\delta e_x}\right) \tag{69}$$

Due to the complex nature of the relationship between ν_{ip} and the phase of the realized change in the relative eccentricity vector, these solutions are computed numerically. Additionally, in order to ensure that three points exist that satisfy Eq. (69), this method nominally requires two orbits to achieve an arbitrary change in the relative state. Considering only the in-plane ROE, combining Eqs. (60-63) yields

$$\boldsymbol{C}\begin{bmatrix}\Delta v_1\\ \Delta v_2\\ \Delta v_3\end{bmatrix} = na\begin{bmatrix}\Delta\delta a\\ \Delta\delta\lambda\\ \Delta\delta e_x\\ \Delta\delta e_y\end{bmatrix} \tag{70}$$

where the subscripts 1, 2, and 3 denote properties of each of the three tangential impulses and the matrix $\boldsymbol{C}$ is given by

$$\boldsymbol{C} = \begin{bmatrix} \frac{2e}{\eta}\sin\nu_1 & \frac{2e}{\eta}\sin\nu_2 & \frac{2e}{\eta}\sin\nu_3 \\ -\frac{3e\sin\nu_1}{\eta}(M_f - M_1) & -\frac{3e\sin\nu_2}{\eta}(M_f - M_2) & -\frac{3e\sin\nu_3}{\eta}(M_f - M_3) \\ \eta\frac{(2+e\cos\nu_1)\cos\nu_1+e}{1+e\cos\nu_1} & \eta\frac{(2+e\cos\nu_2)\cos\nu_2+e}{1+e\cos\nu_2} & \eta\frac{(2+e\cos\nu_3)\cos\nu_3+e}{1+e\cos\nu_3} \\ \frac{\eta}{e}\frac{(2+e\cos\nu_1)\sin\nu_1}{1+e\cos\nu_1} & \frac{\eta}{e}\frac{(2+e\cos\nu_2)\sin\nu_2}{1+e\cos\nu_2} & \frac{\eta}{e}\frac{(2+e\cos\nu_3)\sin\nu_3}{1+e\cos\nu_3} \end{bmatrix} \tag{71}$$

From this formulation, the magnitudes of the in-plane impulses are given in closed-form by

$$\begin{bmatrix}\Delta v_1\\ \Delta v_2\\ \Delta v_3\end{bmatrix} = \frac{na}{|\boldsymbol{C}|}\bar{\boldsymbol{C}}^T\begin{bmatrix}\Delta\delta a\\ \Delta\delta\lambda\\ \Delta\delta e_x\\ \Delta\delta e_y\end{bmatrix} \tag{72}$$

where $|\boldsymbol{C}|$ and $\bar{\boldsymbol{C}}$ denote the determinant and adjugate of $\boldsymbol{C}$, respectively. As in the the near-circular reconfiguration problem, the delta-v cost varies linearly with the required change in the ROE state. Furthermore, the costs associated with changing the in-plane and out-of-plane ROE are decoupled.

The described reconfiguration algorithm is implemented in an iterative scheme in high-fidelity simulations to account for J_2 effects and other geopotential perturbations. This iteration proceeds as follows. First, the orbit of the telescope and occulter spacecraft are initialized from the end condition of the science phase simulation. The initial state of the reconfiguration problem, $\Delta\delta\boldsymbol{\alpha}_i$, is computed by applying the osculating to mean transformation described by Schaub[21] to this relative state. Next, the orbit of the telescope spacecraft is propagated to the start of the next science phase, which is presumed to be centered at the apogee of the second orbit due to the requirements of the reconfiguration scheme. The orbit propagation is performed using the GRACE gravity model GGM01S of order and degree 120.[17] The desired orbit of the occulter spacecraft at the end of the reconfiguration phase is computed by enforcing the initial condition requirements of the science phase. These include: 1) the relative position vector is aligned with the target, 2) the inertial relative velocity perpendicular to the line-of-sight is zero, and 3) the initial separation and drift rates are specified to minimize the deviation from the baseline separation (from Eqs. (19) and (21)). The final state of the reconfiguration problem, $\Delta\delta\boldsymbol{\alpha}_f$, is computed by applying the osculating to mean transformation to this desired relative state. The maneuver sequence for these initial and final states is then computed using the described closed-form algorithm. Next, the orbit of the occulter spacecraft is propagated to the start of the next science phase including the computed maneuvers. The true end state, $\delta\boldsymbol{\alpha}_{end}$, is computed by applying the osculating to mean transformation to the relative state at the end of this propagation. In order to correct for J_2 effects, the maneuver sequence is recomputed with a modified end condition, $\delta\boldsymbol{\alpha}_f^*$, given by

$$\delta\boldsymbol{\alpha}_f^* = \delta\boldsymbol{\alpha}_f + (\delta\boldsymbol{\alpha}_f - \delta\boldsymbol{\alpha}_{end}) \tag{73}$$

and the propagation of the orbit of the occulter spacecraft is repeated. This process is iterated until $\delta\boldsymbol{\alpha}_{end}$ converges to $\delta\boldsymbol{\alpha}_f$. In practice, this iteration scheme nominally converges to sub-meter precision within five iterations. As a final remark, it will be shown in future work that the described closed-form reconfiguration algorithm produces delta-v optimal maneuver sequences through comparison with solutions developed from primer vector theory.[22]

REFERENCE MISSION DESCRIPTION

To illustrate the proposed design strategy, consider a hypothetical mission to image Beta Pictoris (Right ascension: 87^o, Declination: -51^o) for ten science phases with a mDOT formation requiring a 500 km baseline separation. Suppose the formation is deployed in an orbit with a semi-major axis of $24\,500$ km and an eccentricity of 0.72. These values are selected to resemble a geosynchronous transfer orbit (GTO), which has a large apogee radius ($42\,124$ km) and low mechanical energy. Such an orbit can be achieved by a range of launch vehicles. Application of the described formation design strategy provides the initial orbit of the telescope spacecraft specified in Table 2. The expected drift of the argument of perigee and RAAN over the mission lifetime, denoted $\Delta\omega_{total}$ and $\Delta\Omega_{total}$, are included for clarity. The maximum allowable observation duration before the separation deviates by more than 1% of the baseline for the specified orbit is 1.5 hours from Eq. (23). Additionally, the delta-v cost associated with counteracting the secular drift of Ω due to J_2 over the mission lifetime is 42 m/s according to Eq. (59). It will be demonstrated that this is more than an order of magnitude larger than the delta-v cost of the entire mission total when the proposed formation design strategy is implemented. Also, because the value of Ω is expected to deviate by only

Table 2. Initial orbit specification for reference Beta Pictoris Mission

a (km)	e	i (deg)	ω_i (^{o})	Ω_i (^{o})	$\Delta\omega_{total}$ (^{o})	$\Delta\Omega$ (^{o})
24500	0.72	39	88.3	357.3	1.4	-2.6

1.3 degrees from the optimal value, the minimum expected value of $|\gamma|$ over the mission lifetime is approximately 0.9997. From Eq. (41), this reduces the cost associated with the science phase to nearly zero over the entire mission lifetime. It is expected that the delta-v cost associated with each science phase maneuver will be on the order of 1 cm/s or less for each observation.

HIGH-FIDELITY SIMULATIONS

It is now necessary to validate the proposed design strategy through high-fidelity numerical simulations of both science and reconfiguration phases. These simulations will serve two purposes: 1) assess the cost associated with impulsive formation reconfiguration, and 2) demonstrate that the proposed design strategy minimizes the total cost associated with both phases of mission operations.

Science Phase Simulation

The science phase simulation is conducted by first specifying the orbit of the telescope spacecraft. This initial condition is defined either by Table 2 or by the end condition of a reconfiguration phase simulation. The orbit of the occulter spacecraft is specified by enforcing the previously described initial condition requirements for a specified target. The orbits of the telescope and occulter spacecraft are propagated using the GGM01S gravity model. It is assumed that the spacecraft have perfect knowledge of the relative state. Accordingly, the telescope spacecraft applies a continuous thrust that precisely counteracts the differential acceleration perpendicular to line-of-sight throughout the simulation. This control force is numerically integrated to compute the total delta-v cost of the maneuver.

Single Manuever Simulations

In order to characterize the relationship between the costs associated with the science and reconfiguration phases, a set of simulations is conducted that consist of a single science and reconfiguration phase spanning the previously described family of pareto-optimal forced motion control maneuvers. In these simulations, the telescope orbit is initialized with the values presented in Table 2. The occulter orbit is initialized such that the formation is aligned with a target in the TN-plane with the proper initial separation and drift rate. Table 3 gives minimum and maximum values for the time-averaged thrust during the science phase and impulse magnitudes for these simulations. The required continuous control is small enough to enable use of electrospray thrusters,[23] which are suitable for CubeSat deployment and exhibit high specific impulse. Conventional cold gas thrusters can accomplish the required impulsive maneuvers. Figure 11 (left) illustrates the behavior of the science and reconfiguration phase costs with respect to γ in these simulations. Figure 11 (right) illustrates the evolution of the separation over the science phase maneuvers, which does not deviate from the baseline by more than 1% (5 km).

It can be seen that the reconfiguration cost only varies from 0.25 to 0.5 m/s regardless of the value of γ. This is much less than the science phase cost for sub-optimal configurations (small $|\gamma|$). Given

Table 3. Minimum and maximum values of time-averaged continuous thrust and impulse magnitudes for pareto-optimal operations

Min thrust (m/s^2)	Max thrust (m/s^2)	Min impulse (m/s)	Max impulse (m/s)
2.8×10^{-7}	4.2×10^{-4}	0.015	0.1

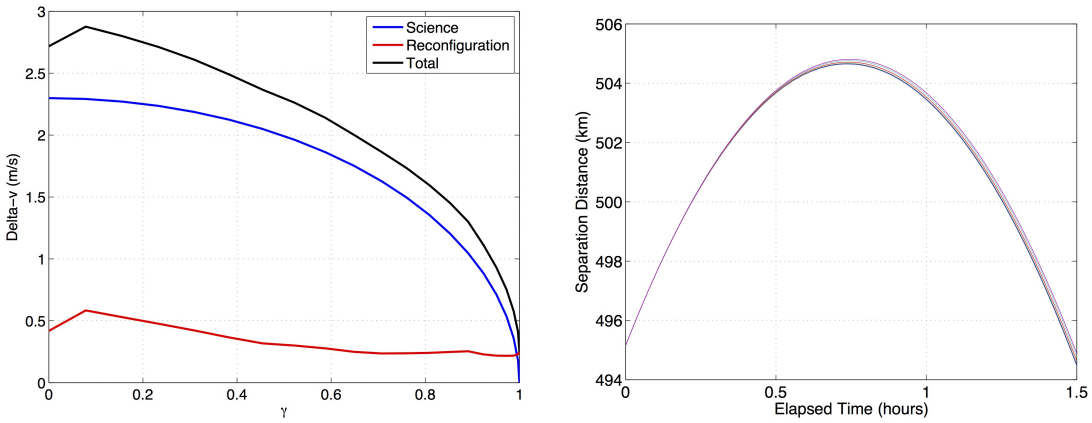

Figure 11. Plot of delta-v costs of science and reconfiguration phases vs γ for reference orbit (left) and evolution of the separation distance during science phase maneuvers (right)

the form of Eq. (67), one would expect the science and reconfiguration costs to be proportional. To illustrate why this is not the case, Figure 12 shows the evolution of $\delta\boldsymbol{\alpha}$ over the course of a single science and reconfiguration phase satisfying $\gamma = 0$. The relative state during the science phase evolves primarily in relative mean longitude and relative eccentricity vector space. It follows from the structure of the control matrix (Eq. (63)) that the control input must be applied primarily in the radial direction. Additionally, the evolution over the course of the science phase is symmetric. The resulting separation between the initial (Figure 12, blue dot) and final (Figure 12, green dot) states is small compared to the total variation of the ROE. The reason for this behavior is that the applied control force evolves linearly over time and is centered about zero at the apogee. Thus, the applied control forces at the beginning and end of the maneuver are equal and opposite. The total change in $\delta\boldsymbol{\alpha}$ over the science phase is therefore primarily driven by second order effects. The reconfiguration cost is governed by the distance between $\delta\boldsymbol{\alpha}_f$ and $\delta\boldsymbol{\alpha}_i$, denoted by green and black dots in Figure 12. For sub-optimal maneuvers, this cost is driven by the evolution of $\delta\boldsymbol{\alpha}$ during the science phase, which is constrained by the previously described symmetry. Finally, because the state evolves along a direct path from the initial to desired state, the reconfiguration maneuvers are evidently optimal.

Figure 11 also shows that the total delta-v cost associated with mission operations is dominated by the reconfiguration cost in the vicinity of the optimal configuration. To illustrate this phenomenon, Figure 13 shows the evolution of $\delta\boldsymbol{\alpha}$ over the course of a science and reconfiguration phase for an optimal configuration satisfying $\gamma = 1$. Because the delta-v cost associated with the science phase is negligible, the relative state does not change. Thus, these maneuvers are characterized by $\Delta\delta\boldsymbol{\alpha}_0 = \Delta\delta\boldsymbol{\alpha}_i$. It follows that the reconfiguration cost in this configuration must be driven by a combination of precession of the absolute orbit ($\Delta\delta\boldsymbol{\alpha}_{J_2}$), and differential effects due to J_2 and

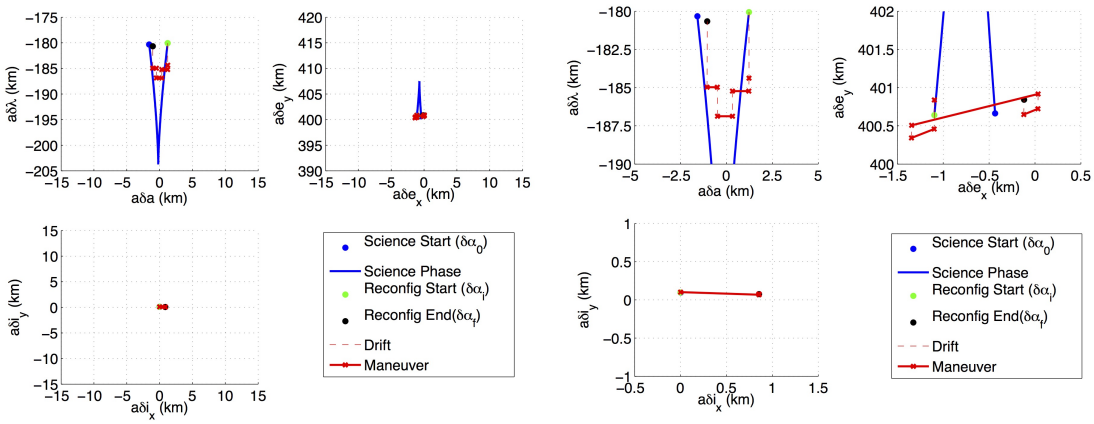

Figure 12. Evolution of the ROE state over one science phase (blue, left) and reconfiguration phase (red, right) for a pareto-optimal maneuver satisfying $\gamma = 0$

Keplerian mechanics. In Figure 13, $\Delta\delta\boldsymbol{\alpha}_{J_2}$ is visualized as the distance between $\delta\boldsymbol{\alpha}_f$ and $\delta\boldsymbol{\alpha}_i$, and differential effects of J_2 and Keplerian mechanics are visualized as the drift of the state between maneuvers (Figure 13, dashed red line). Specifically, drift of the relative eccentricity and inclination vectors is caused only by differential J_2 effects. It is apparent that the out-of-plane reconfiguration cost is driven primarily by $\Delta\delta\boldsymbol{\alpha}_{J_2}$ and that the in-plane reconfiguration cost is driven by both $\Delta\delta\boldsymbol{\alpha}_{J_2}$ and drift of the relative eccentricity vector due to differential J_2 effects. Because the science phase cost is negligible, it is clear that total delta-v cost of nominal operations in the optimal configuration is governed by J_2 effects, which are specified by the location of the science target of interest.

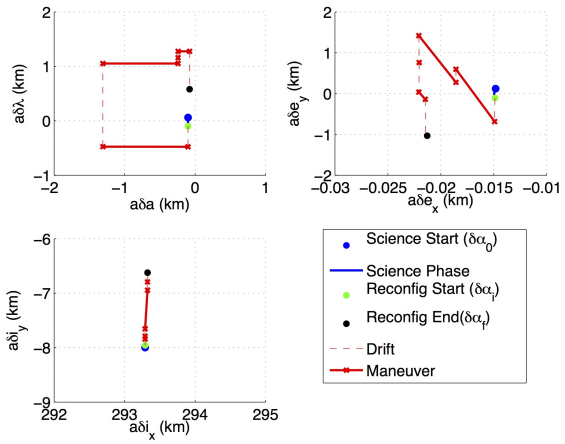

Figure 13. Evolution of the ROE state over the reconfiguration phase (red) for a optimal maneuver ($\gamma = 0$)

Beta Pictoris Mission Simulations

In order to demonstrate the feasibility and optimality of the proposed formation design, the hypothetical mission to image Beta Pictoris for ten 1.5-hour science phases and nine corresponding reconfiguration phases is simulated with the initial orbit described in Table 2. The delta-v cost of

each science and reconfiguration phase over the course of the mission is illustrated in Figure 14. Several conclusions can be drawn from this simulation. First, is is evident from the evolution of

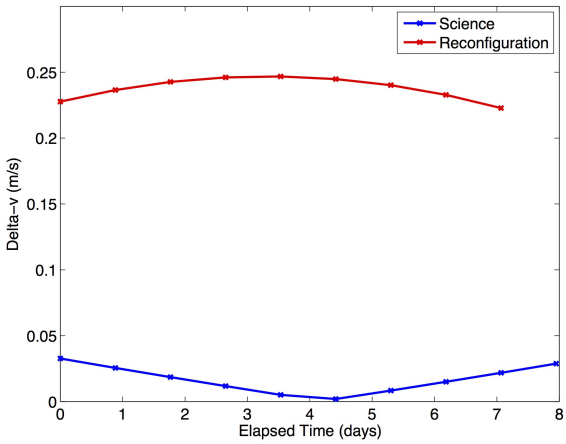

Figure 14. Plot of delta-v costs of science and reconfiguration phases for hypothetical mission to image Beta Pictoris

the science phase cost that optimal alignment is achieved in the middle of the mission lifetime as intended by the formation design. Second, the cost of each of the science and reconfiguration phases over the mission lifetime is very close to the optimal cost shown in Figure 11. This suggests that each maneuver executed during the mission is pareto-optimal. Finally, the total cost of the mission is only 2.31 m/s for 15 hours of total integration time. This is composed of a 2.14 m/s reconfiguration cost and a 0.17 m/s science phase cost. This cost is orders of magnitude less than the delta-v budgets of current small satellite propulsion systems.[23]

In order to fully demonstrate the optimality of the proposed formation design, simulations are conducted with perturbed initial conditions compared to those specified in Table 2. This serves to characterize the sensitivity of the mission cost with respect to orbit injection errors. Specifically, simulations were conducted with errors ranging from 0.5 to 5^o applied individually to ω, Ω, and i. The total delta-v cost of the science and reconfiguration phases for simulations conducted with each of these perturbations is given in Table 4. It can be seen that the delta-v cost for the each

Table 4. Delta-v cost of reference mission (science phase (m/s) / reconfiguration phase (m/s)) subject to orbit injection errors

Error (^{o})	ω	Ω	i
0.5	0.17 / 2.14	0.20 / 2.17	3.80 / 7.62
1	0.17 / 2.14	0.28 / 2.22	7.62 / 20.33
2	0.18 / 2.19	0.53 / 2.46	15.26 / 38.77
5	0.27 / 2.35	1.41 / 4.11	37.97 / 95.18

perturbed mission simulations is no less than the cost associated with the reference mission. Thus, the proposed formation design strategy is delta-v optimal with respect to both the science and reconfiguration phases. It can also be seen that the delta-v cost is insensitive to perturbations of ω and

Ω of less than 5 degrees. However, the cost is very sensitive to perturbations in inclination. Indeed, a perturbation of only 2 degrees increases the mission delta-v cost by more than a factor of 10. The reason for this sensitivity is that perturbing the inclination introduces a radial component of the pointing vector at the apogee of the orbit. This causes a significant change in the relative semi-major axis, which requires costly corrections in the reconfiguration phase. However, these simulations enforce a rigid constraint that the maneuvers are performed about the apogee of the orbit. It may be possible to reduce the sensitivity to inclination by relaxing this assumption. Alternatively, one might consider correcting the inclination before beginning nominal operations. However the cost associated with this correction for the reference orbit, as derived from the Gauss variational equations, is at least 28 m/s per degree of inclination correction. It is apparent from Table 4 that performing such corrections would not reduce the total cost of the mission. As a final remark, the total mission cost associated with an inclination error of 5^o (133 m/s) is still within the total delta-v budgets of current small satellite propulsion systems.[23]

CONCLUSIONS

This paper presented a novel formation design methodology for a miniaturized distributed occulter/telescope in earth orbit which has been demonstrated to minimize the delta-v cost associated with both forced motion control and impulsive reconfiguration. The design strategy is based on the idea that the delta-v cost of forced motion control is minimized by allowing the spacecraft to drift along the line of sight. First, an analytical function of the delta-v cost of forced motion control maneuvers is presented. Considerations of this function and the known secular effects of J_2 were used to select initial values of the argument of perigee and right ascension of the ascending node that miniminize the deviation of the formation from the optimal configuration over the expected mission lifetime. It was demonstrated through high-fidelity simulations that the total delta-v cost of mission operations is driven by J_2 effects when this design strategy is implemented. These effects are specified by the location of the science target of interest. Finally, it was demonstrated that the expected costs associated with nominal operations for this formation are orders of magnitude less than the delta-v budgets of small satellite propulsion systems.

As a preliminary design study, this work introduced a number of simplifying assumptions that must be noted. First, third-body and solar radiation pressure forces are entirely neglected. The presented perturbation study demonstrates that these forces may be comparable to J_2. Second, no consideration is made on the limitations of realistic guidance, navigation, and control systems. Inclusion of such effects (e.g. navigation and maneuver execution errors) may substantially increase operational costs. Also, we have only included costs associated with nominal operations, neglecting formation acquisition and contingency scenarios.

The conclusions of this work call for a number of follow-on studies. First, the impact of third-body and solar radiation pressure forces must be characterized. Second, costs associated with realistic guidance, navigation, and control systems must be addressed. Third, because the costs associated with the optimal configuration derive primarily from J_2 effects, it is worthwhile to investigate the scientific value of targets that can be observed in favorable orbits (e.g. polar orbits that freeze the right ascension of the ascending node). Additionally, an analytical treatment of the reconfiguration cost may allow relaxation of the assumption that the maneuvers must be performed at the apogee. Finally, it is necessary to study the formation design problem for a mission intended to image multiple targets.

Overall, this paper demonstrates that deployment of a miniaturized distributed occulter/telescope

on micro- or nano-satellites in earth orbit is feasible with current propulsion technology provided that the absolute and relative orbits are properly selected. Deployment of such a mission could demonstrate the validity of the distributed occulter/telescope concept and provide a valuable science return at a small fraction of the cost of large-scale platforms. In addition, the proposed formation design strategy can be applied to any distributed telescope in earth orbit.

REFERENCES

[1] W. J. Borucki, D. G. Koch, J. J. Lissauer, G. B. Basri, J. F. Caldwell, W. D. Cochran, E. W. Dunham, J. C. Geary, D. W. Latham, R. L. Gilliland, D. A. Caldwell, J. M. Jenkins, and Y. Kondo, "The Kepler mission: a wide-field-of-view photometer designed to determine the frequency of Earth-size planets around solar-like stars," *Astronomical Telescopes and Instrumentation*, International Society for Optics and Photonics, 2003, pp. 129–140.

[2] C. Marois, B. Macintosh, T. Barman, B. Zuckerman, I. Song, J. Patience, D. Lafrenière, and R. Doyon, "Direct imaging of multiple planets orbiting the star HR 8799," *Science*, Vol. 322, No. 5906, 2008, pp. 1348–1352.

[3] K. R. Stapelfeldt, M. P. Brenner, K. R. Warfield, F. G. Dekens, R. Belikov, P. B. Brugarolas, G. Bryden, K. L. Cahoy, S. Chakrabarti, S. Dubovitsky, *et al.*, "Exo-C: a probe-scale space mission to directly image and spectroscopically characterize exoplanetary systems using an internal coronagraph," *SPIE Astronomical Telescopes and Instrumentation*, International Society for Optics and Photonics, 2014, pp. 91432K–91432K.

[4] D. Spergel, N. Gehrels, J. Breckinridge, M. Donahue, A. Dressler, B. S. Gaudi, T. Greene, O. Guyon, C. Hirata, J. Kalirai, *et al.*, "Wide-field infrared survey telescope-astrophysics focused telescope assets WFIRST-AFTA final report," 2013.

[5] W. Cash, "Detection of Earth-like planets around nearby stars using a petal-shaped occulter," *Nature*, Vol. 442, No. 7098, 2006, pp. 51–53.

[6] S. D'Amico, J.-S. Ardaens, and R. Larsson, "Spaceborne autonomous formation-flying experiment on the PRISMA mission," *Journal of Guidance, Control, and Dynamics*, Vol. 35, No. 3, 2012, pp. 834–850.

[7] M. Landgraf and A. Mestreau-Garreau, "Formation flying and mission design for Proba-3," *Acta Astronautica*, Vol. 82, No. 1, 2013, pp. 137–145.

[8] C. W. T. Roscoe, S. R. Vadali, K. T. Alfriend, and U. P. Desai, "Optimal formation design for magnetospheric multiscale mission using differential orbital elements," *Journal of Guidance, Control, and Dynamics*, Vol. 34, No. 4, 2011, pp. 1070–1080.

[9] S. Seager, W. C. Cash, N. J. Kasdin, W. B. Sparks, M. C. Turnbull, M. J. Kuchner, A. Roberge, S. Domagal-Goldman, S. Shaklan, M. Thomson, M. Lisman, S. Martin, and D. Webb, "Exo-S: A Probe-scale Space Mission to Directly Image and Spectroscopically Characterize Exoplanetary Systems Using a Starshade and Telescope System," *American Astronomical Society Meeting Abstracts*, Vol. 224, 2014.

[10] A. W. Koenig, S. D'Amico, and B. Macintosh, "A Pareto-Optimal Characterization of Small-Scale Distributed Occulter/Telescope Systems," *Optical Engineering+ Applications*, International Society for Optics and Photonics, 2015.

[11] A. P. Hatzes, W. D. Cochran, B. McArthur, S. L. Baliunas, G. A. H. Walker, B. Campbell, A. W. Irwin, S. Yang, M. Kürster, M. Endl, *et al.*, "Evidence for a Long-Period Planet Orbiting Eridani," *The Astrophysical Journal Letters*, Vol. 544, No. 2, 2000, p. L145.

[12] J. R. Graham, P. G. Kalas, and B. C. Matthews, "The Signature of Primordial Grain Growth in the Polarized Light of the AU Microscopii Debris Disk," *The Astrophysical Journal*, Vol. 654, No. 1, 2007, p. 595.

[13] A. Moór, P. Ábrahám, A. Derekas, C. S. Kiss, L. L. Kiss, D. Apai, C. Grady, and T. H. Henning, "Nearby Debris Disk Systems with High Fractional Luminosity Reconsidered," *The Astrophysical Journal*, Vol. 644, No. 1, 2006, p. 525.

[14] T. V. Peters, J. Branco, D. Escorial, L. T. Castellani, and A. Cropp, "Mission analysis for PROBA-3 nominal operations," *Acta Astronautica*, Vol. 102, 2014, pp. 296–310.

[15] D. A. Vallado and W. D. McClain, *Fundamentals of astrodynamics and applications*, Vol. 12. Springer Science & Business Media, 2001.

[16] O. Montenbruck and E. Gill, *Satellite Orbits: Models, Methods and Applications*. Springer Science & Business Media, 2012.

[17] B. D. Tapley, S. Bettadpur, M. Watkins, and C. Reigber, "The Gravity Recovery and Climate Experiment: Mission Overview and Early Results," *Geophysical Research Letters*, Vol. 31, No. 9, 2004.

[18] L. Breger and J. P. How, "Gauss's variational equation-based dynamics and control for formation flying spacecraft," *Journal of Guidance, Control, and Dynamics*, Vol. 30, No. 2, 2007, pp. 437–448.

[19] G. Gaias and S. D'Amico, "Impulsive Maneuvers for Formation Reconfiguration Using Relative Orbital Elements," *Journal of Guidance, Control, and Dynamics*, Vol. 38, No. 6, 2014, pp. 1036–1049.

[20] S. D'Amico and O. Montenbruck, "Proximity operations of formation-flying spacecraft using an eccentricity/inclination vector separation," *Journal of Guidance, Control, and Dynamics*, Vol. 29, No. 3, 2006, pp. 554–563.

[21] H. Schaub and J. L. Junkins, *Analytical Mechanics of Space Systems*. AIAA, 2003.

[22] C. W. T. Roscoe, J. J. Westphal, J. D. Griesbach, and H. Schaub, "Formation establishment and reconfiguration using differential elements in J2-perturbed orbits," *Aerospace Conference, 2014 IEEE*, IEEE, 2014, pp. 1–19.

[23] V. Hruby, "High Isp CubeSat Propulsion," *Interplanetary Cubesat Conference*, 2012.

APPENDIX A: EXTRA EQUATIONS

Elementary Rotation Matrices

$$\boldsymbol{R}_1(\theta) = \begin{bmatrix} 1 & 0 & 0 \\ 0 & \cos\theta & \sin\theta \\ 0 & -\sin\theta & \cos\theta \end{bmatrix} \tag{74}$$

$$\boldsymbol{R}_2(\theta) = \begin{bmatrix} \cos\theta & 0 & -\sin\theta \\ 0 & 1 & 0 \\ \sin\theta & 0 & \cos\theta \end{bmatrix} \tag{75}$$

$$\boldsymbol{R}_3(\theta) = \begin{bmatrix} \cos\theta & \sin\theta & 0 \\ -\sin\theta & \cos\theta & 0 \\ 0 & 0 & 1 \end{bmatrix} \tag{76}$$